

On the Mechanism of the Cathodic Reduction of Anthraquinone to Anthrone

F. Beck and Gabriele Heydecke

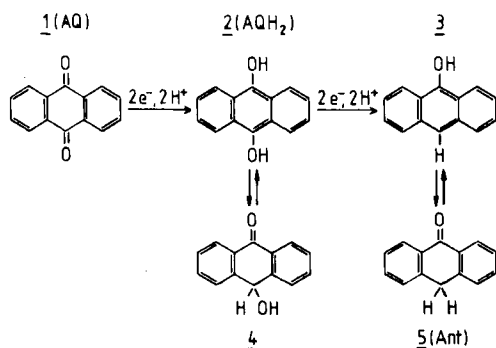
Universität Duisburg GH, FB6-Elektrochemie, Lotharstraße 1, D-4100 Duisburg 1

Electrochemistry / Electrode Kinetics / Transport Properties

The cathodic reduction of anthraquinone in 85% H_2SO_4 at cathodes of glassy carbon or mercury has been investigated. Voltammetric curves exhibit two steps at +0.23 and +0.10 V vs. SHE. The limiting current densities show a ratio between 4:0 via 1:1 to 1:3, depending on the experimental conditions. Experiments at the RRDE indicate two reoxidizable intermediates. — We derive a mechanism from our findings, involving the electrochemical formation of these intermediates, anthraquinone AQH \cdot and anthrahydroquinone AQH $_2$. Both are subject to a bimolecular follow up reaction (disproportionation) to yield AQH $_2$ and anthrone. The rate constants are estimated to be $2 \cdot 10^3$ and $3 \cdot 10^4$ l mol $^{-1}$ s $^{-1}$, respectively. Anthrone is the only reduction product which could be isolated.

1. Introduction

The redox couple benzoquinone/hydroquinone is well known as one of the few examples in organic chemistry to establish a reversible redox system in aqueous or methanolic electrolytes. One two-electron-wave is observed. A ecec or cece mechanism has been found at medium and low pH values, respectively [1, 2]. It is only in anhydrous hydrofluoric acid where a splitting in two one electron waves is observed [3]. However, in aprotic medium, appreciable deviations from reversible behavior occur [4–6]. Moreover, large quinone molecules tend to overoxidation and to over-reduction. Anthraquinone **1** is reduced to anthrahydroquinone **2** and further to anthrone **5** in strongly acid medium [7, 8]. The tautomeric forms oxanthrol **4** and anthranol **3** must be considered in addition, cf. scheme 1.



Scheme 1

Reduction of anthraquinone to anthrone

The two equal voltammetric waves, which are found under some conditions, have been interpreted as two two-electron-waves along scheme 1 [8, 22].

We like to report new results to demonstrate that this mechanism is invalid and must be substituted by a reaction sequence involving two disproportionation steps. Various methods were employed to collect as much information as possible.

2. Experimental

The solvent/electrolyte-system used in most cases was 85 wt% (15.4 M) sulfuric acid, made from 97% H_2SO_4 (Merck, p.a.) and tridistilled H_2O , a verifying compromise on solubilization of an-

thraquinone and reducibility of undissociated H_2SO_4 molecules at higher concentrations [9]. Anthraquinone dissolved up to 20 mM (at 20°C) in this medium.

Anthraquinone (Merck, for synthesis) gave essentially the same results as a sample, crystallized threefold from tetrahydrofuran. Thus it was used without further purification, as it was done with anthrone (Merck, 99%). This holds also for some derivatives of anthraquinone, named in Table 1, which have been provided by BASF company.

Working electrodes were mainly made of glassy carbon, which gave the most reproducible results. In some cases, the mercury drop electrode and an amalgamated silver disc electrode were employed. The counter electrode, made of platinum, was separated by a sintered glass frit. The reference electrode was $\text{Hg}/\text{Hg}_2\text{SO}_4/1$ M H_2SO_4 , its potential vs. SHE being +674 mV. Potentials are denoted as U_s .

Voltammetric measurements were made with conventional experimental setups:

Polarography (conventional and differential pulse mode) with a Polarecord E 605 (Metrohm).

Cyclic voltammetry with a cylindrical glassy carbon electrode, $A = 1.5$ cm 2 (Function generator AMEL 568, Potentiostat RDE 3 (PINE Instruments Co)).

Voltammetry with the rotating disc electrode (RDE) and rotating ring disc electrode (RRDE) from PINE Instruments was performed with the same circuit.

Chronoamperometry was realized with a stationary glassy carbon disc electrode. The circuit involved a potentiostat AMEL 551, a square pulse generator AMEL 565, a transient recorder VUKO 22-4, and an oscilloscope Gould Advance.

Preparative electrolysis at a constant potential in the region of the overall limiting current was performed with a rotating glassy carbon cylinder electrode ($A = 6.3$ cm 2 , 800 rpm). A cylindrical ceramic diaphragm separated the anode compartment where a platinum counter electrode was dipping in pure 85% H_2SO_4 .

All measurements were made at 25°C, if not stated otherwise. The electrolyte was purged 20 minutes with pure N_2 prior to each measurement.

3. Results

3.1. Polarography

Conventional polarographic curves have been measured in the range of 0.1–20 mM AQ. Two waves of equal intensity are observed at low concentrations up to 1 mM. The diffusion limited current densities for $c = 1$ mM were both 31 $\mu\text{A cm}^{-2}$. At higher concentrations, the second wave grows much more faster than the first, leading to a proportion 1:10 at 20 mM. Polarographic maximum behaviour is clearly indicated by a sudden break down of the current at $U_s = -1.2$ V prior to the basic curve, which rises at -1.3 V in 85% H_2SO_4 [9].

Half wave potentials of both waves in the lower concentration region are collected in Table 1 for AQ and some of its derivatives.

For comparison, the potentials for AQ for the one step reduction in methanolic electrolytes using the rotating disc electrode have been included.

Table 1
Polarographic half wave potentials for anthraquinone and some of its derivatives in 85% H₂SO₄ at 25°C. *c* = 1 mM. Potentials ^H*U* vs. SHE. Values for AQ in methanolic electrolytes for comparison

	^H <i>U</i> _{1/2} /V 1. wave	^H <i>U</i> _{1/2} /V 2. wave
Anthraquinone	+0.23	+0.10
2-Methylanthraquinone	+0.23	+0.10
2-Ethylanthraquinone	+0.23	+0.10
*2-Chloroanthraquinone	+0.25	+0.16
*2-Aminoanthraquinone	+0.26	+0.22
AQ, 0.1 M HClO ₄ /1 M NaClO ₄ in MeOH	+0.04	
AQ, 0.01 M MeCOOH/ 0.01 M MeCOONa/1 M NH ₄ NO ₃ in MeOH	-0.26	

* Poor separation of the two waves.

Similar values have been found as peak potentials with differential pulse polarography. The positive shift for the last two AQ derivatives reflects the electron supply by the two substituents. The AQ potentials in the three electrolytes correspond to pH-values of 6, 1 and -2.5. The first two have been measured with a glass electrode.

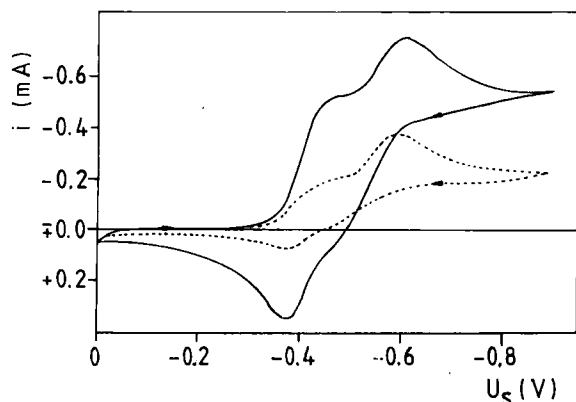


Fig. 1
Rapid cyclic voltammetry at a glassy carbon electrode (*A* = 1.5 cm²). 10 mM AQ in 85% H₂SO₄, 25°C
— *v*_s = 1000 mV s⁻¹; - - - *v*_s = 200 mV s⁻¹
The 15th cycle is drawn. Basic curve has been subtracted

3.2. Cyclic Voltammetry

Stationary electrodes of glassy carbon have been employed for cyclic voltammetry with voltage scan rates from *v*_s = 20 to 1000 mV s⁻¹. Fig. 1 gives two typical examples. Two peaks are observed. The first peak grows much more faster than the second one. Reversibility increases strongly with increasing *v*_s. Peak height ratio is inverted on reversal scan for high *v*_s.

The observed behavior is in qualitative agreement with a ecec mechanism, where the second reaction product is electrochemically inactive. The normalized peak current density *j*_p/*v*_s^{1/2} is fairly constant for the first peak, while it is not for the second.

3.3. Voltammetry at the Rotating Disc Electrode (RDE)

Fig. 2 shows clearly two steps in the voltammetric curves at the RDE, where the rotation speed *n* has been monitored between 400

and 4000 rpm. The half wave potentials correspond to the polarographic values. Logarithmic analysis of the first wave, especially at low concentrations and high rotation speeds, leads exactly to an electron number of *z* = 1. The second wave grows faster than the first one with increasing *n*. Moreover, the ratio of both limiting current densities *j*_{lim,2}/*j*_{lim,1} increases with increasing concentration of the starting material, as it is demonstrated in Fig. 3.

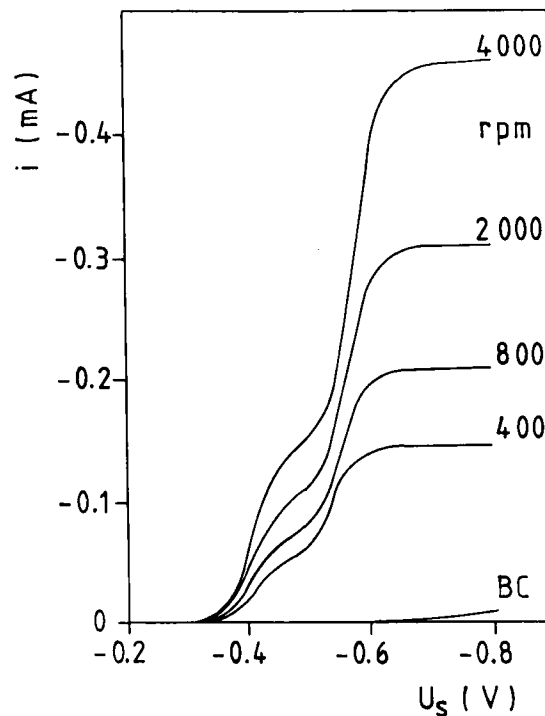


Fig. 2
Quasi steady state current voltage curves at the rotating disc electrode (glassy carbon). Rotation speed (min⁻¹) is indicated at each curve. 10 mM AQ in 85% H₂SO₄, 25°C, *v*_s = 5 mV s⁻¹.
BC = basic curve

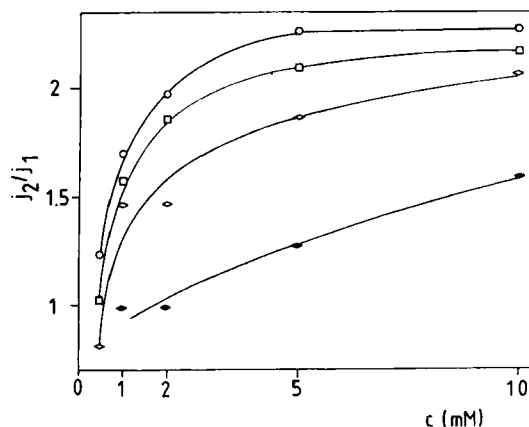


Fig. 3
Ratio of the limiting current densities of the second and of the first step *j*₂/*j*₁ versus concentration of AQ in 85% H₂SO₄ for voltammetric measurements as in Fig. 2. Parameter is the rotation speed:

- 4000 rpm
- 2000 rpm
- ◇—◇ 800 rpm
- ◆—◆ 400 rpm

While the Levich-plots of the overall limiting current densities give straight lines through the origin for all concentrations, the same plots for the first step exhibit strong deviations at low rotation

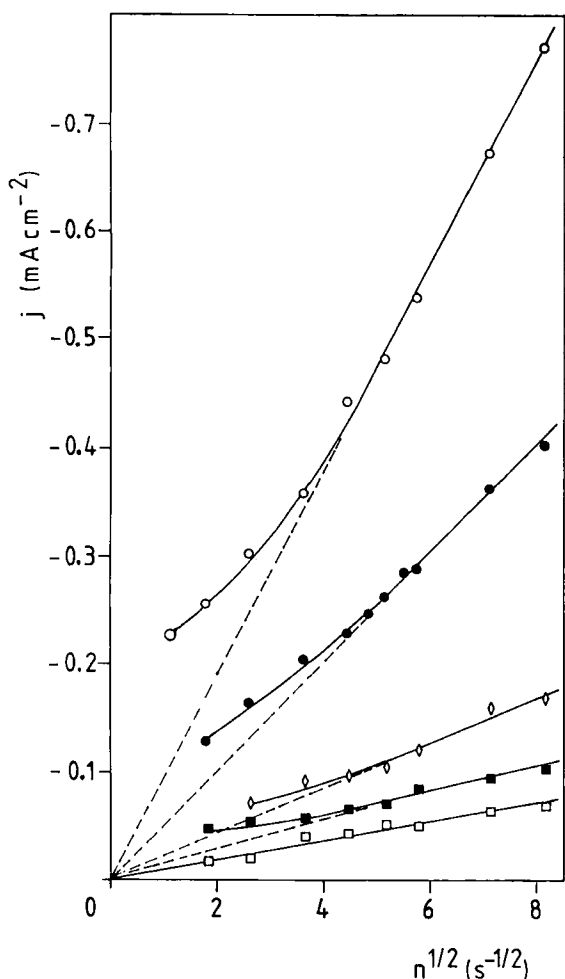


Fig. 4
Lewich plot of the limiting current densities of the first step at the RDE (glassy carbon) versus the square root of the rotation speed n (s^{-1}). Parameter is the concentration of AQ in 85% H_2SO_4 :

- 10 mM
- 5 mM
- ◇—◇ 2 mM
- 1 mM
- 0.5 mM

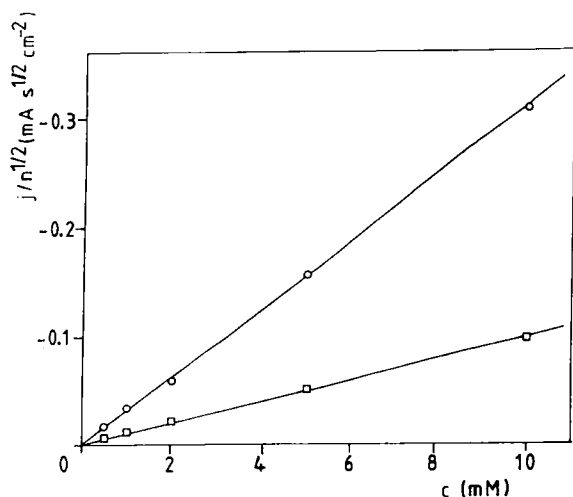


Fig. 5

Normalized plot of limiting current densities $-\frac{j}{\sqrt{n}}$ vs. c (AQ in 85%

- H_2SO_4 , RDE glassy carbon).
- Sum of both steps
- First step

speeds and high concentrations, as shown in Fig. 4. This leads to the conclusion that under these conditions a current multiplying chemical reaction of the electrochemically generated first intermediate occurs, feeding back the starting material to the electrode surface.

A normalized plot of the limiting current densities of the first step and of the overall step versus the concentration is given in Fig. 5. The deviations mentioned above are not visible in this case. The slope of these curves leads to a well averaged value for the product $z \cdot D^{2/3}$ according to the Levich equation

$$j_{lim} = 1.56 z F D^{2/3} \nu^{-1/6} n^{1/2} c \quad (1)$$

The current voltage curves have been measured at 40 and 60°C in addition. If D increases with temperature according to

$$D = D_0 \exp(-E_a/RT) \quad (2)$$

a modified Arrhenius plot

$$\ln(j_{lim} \cdot \nu^{1/6}) = \text{Const} - \frac{2}{3} \frac{E_a}{RT} \quad (3)$$

leads to straight lines, from which $E_a = 36$ kJ/mol has been deduced. The current rises with about 7%/°C, much more than for pure diffusion (1%/°C). The separation of the two steps becomes poor at elevated temperatures and finally one four electron step has been found. Polarographic measurements in concentrated H_2SO_4 in the range of 8–32°C led formerly to a temperature coefficient of the limiting current of 3.4% per °C [10]. It must be concluded that a mixed diffusion and kinetic control of the limiting current is operative.

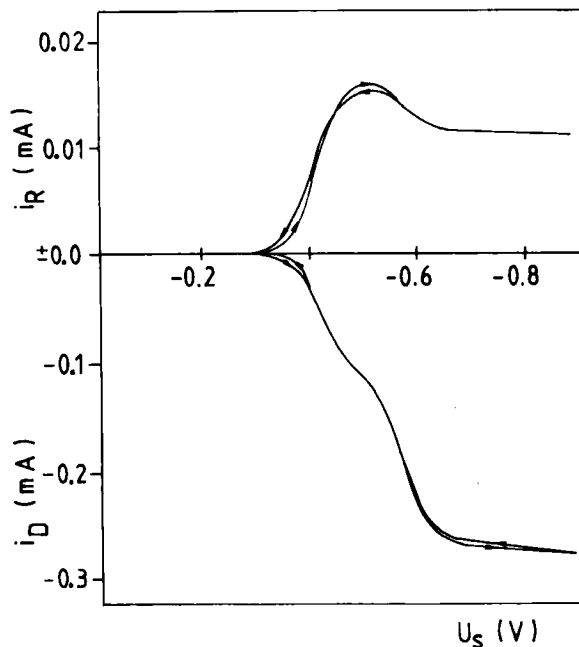


Fig. 6

Typical example for the RRDE measurements. Lower curve: Current voltage curve at the GC disc. Same conditions (10 mM AQ in 85% H_2SO_4 , 2000 rpm) as in Fig. 2. Upper curve: Current time curve at the Pt-ring at $U_s = +0.4$ V

3.4. Voltammetry at the Rotating Ring/Disc-Electrode (RRDE)

The experiments with the RRDE were performed with glassy carbon as the disc material and platinum as the ring material. The three characteristic radii are $r_1 = 0.2080$ cm, $r_2 = 0.3585$ cm and $r_3 = 0.4145$ cm. The relatively large gap between disc and ring

invalidizes the theoretical relationship [11,12] to calculate the transfer efficiency N_0 . The experimental value, measured with 1 mM $K_3Fe(CN)_6/0.1$ M Na_2SO_4 in water, was found to be $N_0 = 0.158$.

Typical voltammetric curves are reproduced in Fig. 6. The ring current at $U_s = +0.4$ V rises up to a maximum in the course of the first wave (at the disc) and it decreases again in the course of the second wave. However, it never regains zero, but it is fixed at

Table 2
Collection efficiencies N at the RRDE (25°C)

n rpm	N_1 (10 mM)	N_{tot} (10 mM)	N_1 (5 mM)	N_{tot} (5 mM)
4000	0.153	0.044	0.141	0.030
3000	0.149	0.039	0.127	0.027
2000	0.125	0.036	0.114	0.022
1600	0.127	0.028	0.118	0.021
1200	0.115	0.022	0.096	0.020
800	0.104	0.015	0.078	0.014
400	0.070	0.009	—	0.005

Table 3
Temperature effect for N_1 and N_{tot} in 10 mM solutions

N	rpm	25°C	40°C	60°C
N_1	4000	0.153	0.068	—
	2000	0.125	0.040	—
	1200	0.115	0.022	—
N_{tot}	4000	0.044	0.009	0.005
	2000	0.036	0.004	0.002
	1200	0.022	0.002	0.001

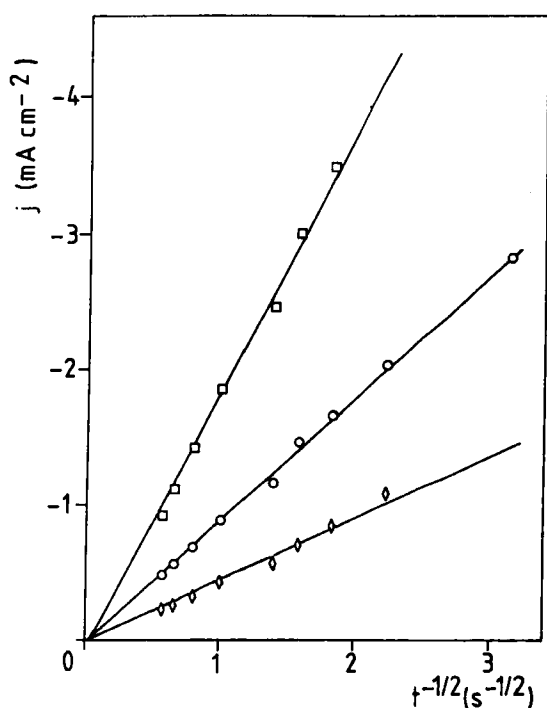


Fig. 7

Chronopotentiometric curves at glassy carbon (Cottrell plot j vs. $t^{-1/2}$) for three concentrations of AQ in 85% H_2SO_4 . Potentiostatic switch of potential to $U_s = -750$ mV.

□—□ 10 mM
○—○ 5 mM
◇—◇ 1 mM

a constant limiting value in the region of the second plateau (at the ring). The collection efficiencies N are appreciably lower than N_0 (with a stable redox system) which is due to the fact, that the species are partially consumed by a chemical reaction on their way from the disc to the ring.

Table 2 compiles the collection efficiencies for the intermediates, generated in the first and the overall plateau of the current voltage curve at the disc for two concentrations:

$$N_1 = j_{max,R}/j_{lim1,D}$$

$$N_{tot} = j_{lim,R}/j_{lim,tot,D}$$

It can be concluded from these data, that the chemical reaction consuming intermediates generated in the second plateau, is much faster than for those in the first step. At higher temperatures the reaction rates increase further, and N decreases even more. This is shown in Table 3 for some characteristic examples.

3.5. Chronoamperometric

A stationary glassy carbon disc electrode was polarized in a non-stirred solution by a potential step up to the region of the second limiting current density. The current time curves were analyzed according to Cottrell's equation. Fig. 7 gives the adequate plot of the data. For three concentrations, three straight lines are obtained, starting from the origin. The slope of these lines yields the same product $zD^{1/2}$ as in the Ilcovič equation.

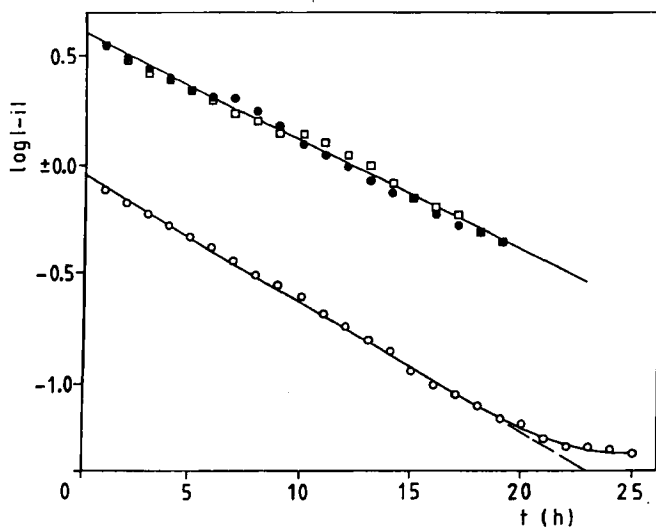


Fig. 8

Semilogarithmic current time curves for the potentiostatic electrolysis of AQ at a rotating GC-electrode. Potential was held in the region of overall limiting current density.

□—□ } $c_0 = 10$ mM, 2 parallel runs
●—● }
◇—◇ } $c_0 = 2$ mM

3.6. Electrolysis at Constant Potential

Preparative electrolysis was performed at a rotating glassy carbon cylinder electrode (400 rpm). The potential was held at $U_s = -0.7$ V, in the region of the overall limiting current density. The anode was separated by a porous diaphragm. Fig. 8 shows the current time curves in a semilogarithmic plot for three independent runs. From the negative slope of the straight lines, the number of electrons for the overall process can be easily derived [13]. Assuming a current efficiency of 1.00, the result is the following:

$$z = 4.09 \text{ for the experiment with } c_0 = 2 \text{ mM}$$

$$z = 4.25 \text{ for the experiments with } c_0 = 10 \text{ mM.}$$

It is clear from that finding, that the overall reduction must be written as



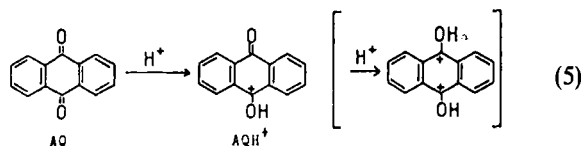
This was confirmed by working up the solution after the electrolysis by dilution with icewater 1:13 and filtration with a sintered glass filter. NMR and IR spectrum revealed anthrone and traces of non reacted anthraquinone. The yield was 87%.

4. Discussion

The results outlined in the last section show anthrone to be the final product of the electroreduction of anthraquinone. It is anodically inactive in the whole potential region used for our experiments ($U_s = -1,0 \dots +0,4$ Volt). The following findings are indicative for the fact that chemical steps (other than protonation and dehydration) are involved in the reaction sequence:

- high temperature coefficient of limiting current densities (7%/°C)
- current amplification of the first cyclovoltammetric peak
- current amplification of the first or the second voltammetric step at the RDE, depending on the experimental conditions
- strong variation of the transfer coefficient N with the rotation speed n in the RRDE experiments.

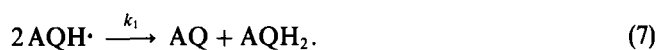
Anthraquinone will be protonated in the strongly acid medium:



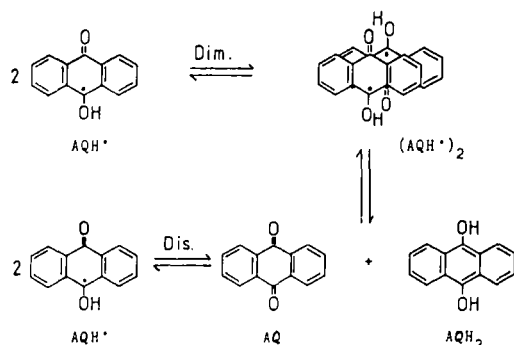
The protonated anthraquinone will be initially reduced to the semiquinone radical:



This radical is known to be subject of a relatively fast disproportionation reaction [14,15] according to Eq. (7) and to scheme 2:



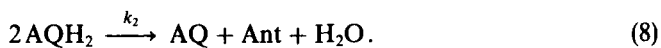
This means that the reaction is bimolecular to yield the products AQ and AQH₂ directly or through a dimer as an intermediate



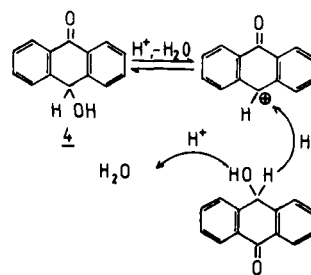
Scheme 2

Disproportionation of Anthrasemiquinone radical

Reaction (7) yields anthrahydroquinone as an intermediate and regenerates AQ which enters again into the primary steps (5) and (6). Thus the current of the first step will be amplified. Moreover, hydroquinone undergoes itself a second disproportionation reaction:



Matthews observed the rapid formation of anthraquinone and anthrone from anthrahydroquinone in cold concentrated sulfuric acid [16]. No quantitative kinetic evaluation of this reaction seems to be available. Scheme 3 represents a possible mechanism, taking general aspects of organic chemistry into account [17]. The reaction starts with a protonation/dehydration of the tautomeric oxanthrol. It follows a hydride shift from a second molecule as the most important step:

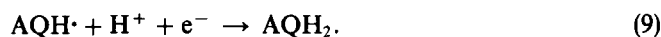


Scheme 3

Disproportionation of anthrahydroquinone

According to our results, this chemical step (8) seems to be even faster than (7), see below. A further multiplication of the current in step one is the consequence.

In the course of the second step, a further reduction of the semiquinone radical occurs:



AQH₂ is formed, which undergoes rapid disproportionation according to Eq. (8). Once again, the current is amplified appreciably if the concentration of AQH₂ is high enough. For this reaction path no electrochemical formation of Ant is necessary. It is highly improbable indeed, that a carbonyl group (in 4) or a C–O-bond (in 2) can be reduced at the relatively positive electrode potentials of the second step.

The reaction mechanism Eqs. (5)–(9) opens the possibility for a complete understanding of all experimentally facts. Firstly, the ratio of the two steps will be discussed. Thereafter, the rate constants k_1 and k_2 will be derived from the RRDE experiments.

Concerning the ratio of the two voltammetric steps, the most simple case is a pure electrochemical mechanism corresponding to the two one electron reactions Eqs. (6) and (9). This is observed at very low concentrations of AQ, leading to low concentrations of the intermediates AQH[·] and AQH₂. The bimolecular reactions (7) and (8) do not proceed at an appreciable extent within the diffusion layer. This has been found for the polarographic curves at low concentrations, cf. section 3.1 and our former results [18].

As the reaction layer thickness ϱ for the bimolecular reactions Eqs. (7) and (8) does not only decrease with increas-

ing k , but also with increasing c , ϱ becomes smaller than the diffusion layer thickness δ at higher concentrations of AQ or AQH[•] (and therefore with higher current density). The amplification of the first peak in Fig. 1 at high v_s and of the limiting current density of the first step in Fig. 4 at high concentrations and low rotation speeds becomes qualitatively understandable.

In the second step, AQH₂ is generated electrochemically and undergoes rapid disproportionation. The reaction layer for this reaction seems to be permanently inside the diffusion layer under our experimental conditions.

At high concentrations of AQ, high current densities, high temperatures and small rotation speeds, the intermediate AQH[•] may accumulate in front of the electrode to such an extent, that the whole reduction runs via Eqs. (6)–(8), and the first step involves four electrons. However, as the rate constant k_2 is ten times larger than k_1 (see below), the normal case is, that the second step is amplified to a greater extent than the first one, and $j_{\text{lim},2}/j_{\text{lim},1} = 1 \dots 3$ is the consequence, cf. Fig. 3.

The chronoamperometric experiment leads to a high initial concentration of AQH[•] (due to the high initial current density), and the complete reaction sequence (6)–(9) ($z = 4!$) runs smoothly. For potentiostatic electrolysis under controlled potential, z is found to be 4 as well. In this case, we have a long term experiment, and even if the intermediates would escape from the diffusion layer, they have ample time in the bulk of the electrolyte to disproportionate slowly, thus restoring the concentration level of AQ to an extent corresponding to an overall 4 e-reaction.

The two rate constants k_1 and k_2 of the reactions Eqs. (7) and (8) can be derived from the collection efficiencies N_0 and N at the RRDE. N_0 has been measured to be 0.158 (cf. sect. 3.4). If the reoxidizable intermediate is consumed by a second order reaction, only a fraction $\frac{N}{N_0}$ reaches the ring, and the following equation can be used [19, 20]:

$$\left(\frac{N_0}{N} - 1\right) = k \cdot N_0 \cdot c_1 \cdot b \cdot \left(\frac{v}{D}\right)^{1/3} \cdot \frac{1}{n}. \quad (10)$$

Plotting $\frac{N_0}{N} - 1$ (taken from Table 2) versus the inverse rotation speed n leads to straight lines through the origin, as it is shown in Fig. 9. From the slope of these lines, taking $b = 0.1$ [19], $v = 0.12 \text{ cm}^2 \text{ s}^{-1}$ [21] and $D = 5 \cdot 10^{-7} \text{ cm}^2 \text{ s}^{-1}$ (see below), the following second order rate constants can be calculated:

$$k_1 = 2 \cdot 10^3 \text{ l mol}^{-1} \text{ s}^{-1}$$

$$k_2 = 3 \cdot 10^4 \text{ l mol}^{-1} \text{ s}^{-1}.$$

The concentration c_1 of the intermediate has been arbitrarily taken as half of the concentration of AQ. The diffusion coefficient follows from our measurements as an average value according to Table 4.

Our mechanism disagrees with the 2×2 electron scheme put forward by other authors [8, 22]. These authors have found a current voltage curve with two equal steps at

60–90°C with a rotating graphite cathode. Our mechanism does not exclude this current voltage behavior (1 + 1 or 2 + 2 electron step), but it is a special case of a more general mechanism. Two polarographic steps with various ratios $j_{\text{lim},1} : j_{\text{lim},2}$ have been observed in glacial acetic acid/10% H₂SO₄ [23].

Table 4
Calculation of diffusion coefficient

Method	Results	z	$D/\text{cm}^2 \text{ s}^{-1}$
Polarography, 1. step	$z_1 \cdot D^{1/2} = 7.3 \cdot 10^{-4} \text{ cm s}^{-1/2}$	1	$5.3 \cdot 10^{-7}$
Rotating disc electrode, overall step	$z \cdot D^{2/3} = 5 \cdot 10^{-5} \text{ cm}^{4/3} \text{ s}^{-2/3}$ (from Fig. 5)	4	$2.3 \cdot 10^{-7}$
Chronopotentiometry	$z \cdot D^{1/2} = 3.3 \cdot 10^{-3} \text{ cm s}^{-1/2}$ (from Fig. 7)	4	$6.8 \cdot 10^{-7}$

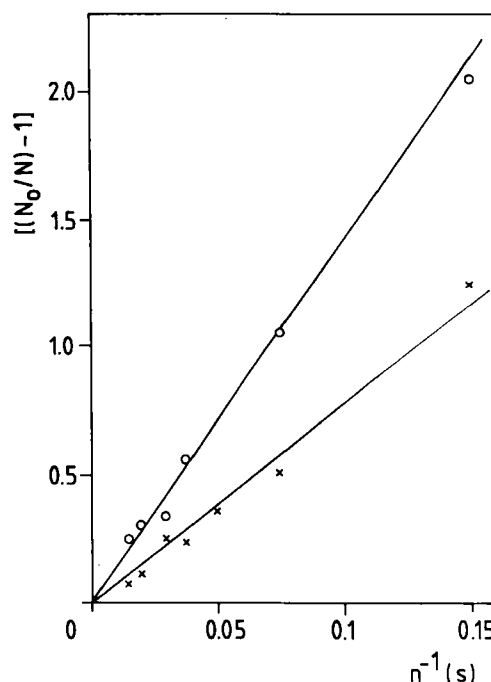


Fig. 9
Kinetic evaluation of the RRDE experiment for 10 mM AQ in 85% H₂SO₄, cf. text.
×—× first step
○—○ second step

5. Practical Conclusions

The electroreduction of anthraquinone to anthrone in 85% H₂SO₄ has been proposed [8, 22, 24] as an alternative to the industrial synthesis with iron as reductant, circumventing the copious by-product ironsulphate. The intermediate anthrahydroquinone cannot be isolated under these conditions. However, it reacts rapidly (in its oxanthrol form **4**) with glycerine to yield quantitatively benzanthrone, an important dye intermediate [24].

Anthraquinone has been proposed as a negative active mass in secondary batteries [25–29]. However, it is extremely doubtful in the light of our new mechanism, that good reversibility can be achieved in acid solutions due to

the possible side reaction (9). Fig. 4 in [28] seems to indicate a loss of capacity of about 5% per cycle.

Provision of some derivatives of anthraquinone by BASF Aktiengesellschaft, Ludwigshafen, is gratefully acknowledged.

References

- [1] K. J. Vetter, *Z. Elektrochem.* **56**, 797 (1952).
- [2] J. M. Hale and R. Parsons, *Trans. Farad. Soc.* **59**, 1429 (1963).
- [3] J.-P. Masson, J. Devynck, and B. Trémillon, *J. Electroanal. Chem.* **64**, 175 (1975).
- [4] L. Jeftic and G. Manning, *J. Electroanal. Chem.* **26**, 195 (1970).
- [5] B. R. Eggins and J. Q. Chambers, *J. Electrochem. Soc.* **117**, 186 (1970).
- [6] V. J. Koshy, V. Swayambunathan, and N. Periasamy, *J. Electrochem. Soc.* **127**, 2761 (1980).
- [7] H. Lund, in: "The Chemistry of the Hydroxylgroup", p. 274, ed. E. Patai, Interscience Publishers Inc., New York 1971.
- [8] Ch. Cominellis and E. Plattner, *J. Appl. Electrochem.* **15**, 771 (1985).
- [9] F. Beck, *Electrochim. Acta* **17**, 2317 (1972).
- [10] S. R. Porter, J. V. Jennings, A. Dotson, and W. J. Ogleby, *Proc. Soc. Analyt. Chem.* **10**, 278 (1973).
- [11] W. J. Albery and S. Bruckenstein, *Trans. Faraday Soc.* **62**, 1932 (1966).
- [12] W. J. Albery and M. L. Hitchman, "Ring disc electrodes", Clarendon Press, London 1971.
- [13] L. Meites, *Pure Appl. Chem.* **18**, 35 (1969).
- [14] S. K. Wong, W. Sitnykh, and J. K. S. Wan, *Can. J. Chem.* **50**, 3052 (1972).
- [15] I. V. Khudyakow and V. A. Kuzmin, *Usp. Khim. (Russ. Chem. Rev., Engl.)* **44**, 801 (1975).
- [16] M. A. Matthews, *J. Chem. Soc. (London)* **1926**, 237.
- [17] H. J. Schäfer, private communication 1. 7. 1986.
- [18] F. Beck, *Ber. Bunsenges. Phys. Chem.* **77**, 353 (1973).
- [19] H. Schurig and K. E. Heusler, *Z. analyt. Chem.* **224**, 45 (1967).
- [20] H. Gerischer, I. Mattes, and P. Braun, *J. Electroanal. Chem.* **10**, 553 (1965).
- [21] Landolt Börnstein, *Tables*, Vol. 5a, 6. Edition, Springer, Berlin.
- [22] J. Bersier, private communication 4/1985.
- [23] L. Starka, A. Vystrčil, and B. Starkowa, *Coll. Czech. Chem. Commun.* **23**, 206 (1958).
- [24] *Europ. Pat.* 0022062 (Ciba Geigy, 1980); J. Bersier, H. Jäger, and H. Schwander.
- [25] H. Alt, H. Binder, A. Köhling, and G. Sandstede, *J. Electrochem. Soc.* **12**, 1950 (1971).
- [26] H. Alt, H. Binder, A. Köhling, and G. Sandstede, *Electrochim. Acta* **873** (1972).
- [27] H. Binder, A. Köhling, and G. Sandstede, *Ber. Bunsenges. Phys. Chem.* **80**, 66 (1976).
- [28] H. Binder, R. Knödler, A. Köhling, G. Sandstede, and G. Walter, *Proc. of the Power Sources Symposium*, 643 (1978).
- [29] G. Matricali, M. M. Dieng, J. F. Dufeu, and M. Guillou, *Electrochim. Acta* **21**, 943 (1976).

(Eingegangen am 13. August 1986, E 6330
endgültige Fassung am 29. September 1986)

Semiconduction in the Liquid Tl—SbTlX₃ System (X: Te, Se)

O. Uemura, H. Matsuda, and T. Satow *)

Department of Chemistry, Faculty of Science, Yamagata University, Yamagata 990, Japan

Electrical Properties / Magnetic Properties / Semiconductors / Thermoelectric Power

The electrical conductivity, the magnetic susceptibility, and the thermoelectric power of the liquid Tl—SbTlTe₃ and Tl—SbTlSe₃ systems have been obtained as a function of temperature and composition from near the liquidus temperature up to about 1200 K. The telluride system exhibits a sharp minimum in electrical conductivity and a maximum in diamagnetic susceptibility around the composition of 80 mol% Tl. On the other hand, in the selenide system the conductivity changes little up to 66.7 mol% Tl(SbTl₃Se₃), and it rapidly increases with increasing Tl content above that stoichiometric composition. The thermoelectric power of both systems shows a change in sign around the respective compositions. The electronic properties of these liquid systems are discussed in the light of current transport theories employed in the amorphous and liquid semiconductors.

1. Introduction

When adding Tl metal to molten Te, Se and some chalcogenides, the electrical conductivity of the system reduces gradually and a further addition of Tl gives rise to a sharp minimum in conductivity at a given composition due to the formation of the stable "clusters" with strong attractive forces between unlike atoms [1, 2]. This type of compound formation often appears at a composition, where the Tl atoms can reasonably be expected to be univalently ionized from the valence requirements of the other atoms in the mixture as the cases at the composition Tl₂Te in the liquid Tl—Te system [2] and AgTl₃Te₂ in the liquid Tl—AgTlTe₂ system [3].

On the other hand, a recent investigation of the liquid Tl—BiTlTe₃ system has revealed that the conductivity mini-

mum is not observed at the composition of BiTl₃Te₃ but around the composition of BiTl₅Te₃ [4]. This suggests that Bi also changes its valence with alloy composition as well as Tl in this system.

The present paper describes the experimental results of some electronic properties in the liquid Tl—SbTlTe₃ system. Since Sb and Bi belong to the V_b group in the periodic table and both are chemically very similar, it may be considered that the conductivity minimum in the system appears around the composition of SbTl₃Te₃ by analogy with the Tl—BiTlTe₃ system. However, in the molten state there exists, although small, a significant difference in the bond strength against Te atoms between Sb and Bi atoms, for example Bi—Te bonds in Bi₂Te₃ are destroyed to a large extent on melting and molten Bi₂Te₃ behaves as a metal rather than a semiconductor, whereas, Sb₂Te₃ remains semi-conductive even in the molten state just above the melting point [5]. This gives us the hint that the liquid Tl—SbTlTe₃

*) Author to whom correspondence should be addressed.